Synthesis and Magnetic Property of Multiferroic BiMnO3 Nanoparticles in the Pores of Mesoporous Silica

Synthesis and Magnetic Property of Multiferroic $BiMnO_3$ Nanoparticles in the Pores of Mesoporous Silica

Takayuki Tajiri, Manabu Harazono[1], Hiroyuki Deguchi[1], Masaki Mito[1], Atsushi Kohno, and Shigemi Kohiki[1]

Faculty of Science, Fukuoka University, Fukuoka 814-180, Japan
[1]Faculty of Engineering, Kyushu Institute of Technology, Kitakyushu 804-8550, Japan

The mesoporous silica material SBA-15 was prepared with control pore size for use as a nanoparticle synthesis template. The X-ray diffraction results show that the nanopores were ordered in a hexagonal structure. The pore size was controlled by the synthesis conditions. Nanoparticles of the multiferroic compound $BiMnO_3$ with an average size of about 14 nm were successfully synthesized in the pores of SBA-15, and their magnetic roperties were investigated. The prepared $BiMnO_3$ nanoparticles showed both antiferromagnetic and ferromagnetic behavior, whereas $BiMnO_3$ bulk crystals consistently showed ferromagnetic behavior. The prepared $BiMnO_3$ nanoparticles exhibited unique magnetic size effects: the appearance of antiferromagnetic behavior and the coexistence of antiferromagnetic and ferromagnetic components.

1. Introduction

It is interesting to investigate nano-scale materials since the effects of quantum confinement in nanostructures and the significant influence of the surface state yield remarkable properties as compared with those of bulk crystal. The physical properties depend on the size of nano-scale materials. To investigate the specific structure and properties of nanoparticles, various preparation methods, such as the chemical precipitation method, coating with polymer, sputtering and depositing, have been developed, and many interesting phenomena have been observed and reported so far. In addition, nanoparticles have been synthesized in porous materials and mesoporous silica, such as MCM-41 and SBA-15, and their size effects have been investigated. The mesoporous silica material MCM-41[1,2] and SBA-15[3–5] have one-dimensional pores, which are separated by thick uniform silica walls, and the size distribution is small. SBA-15 has a well-ordered two-dimensional hexagonal mesoporous structure with a pore diameter of about 5 –30 nm, and the pore size and wall thickness can be controlled by the synthesis conditions.[3–5] Since the synthesis of nanoparticles in the pores of SBA-15 allows the control of the particle size, SBA-15 is suitable for use as a template for nanoparticle fabrication to investigate size effects etc. From the viewpoint of the magnetic properties, since mesoporous silica such as MCM-41 and SBA-15 are nonmagnetic, they can act as templates for magnetic nanoparticle fabrication.[6–11] Magnetic nanoparticles generally exhibit many interesting behaviors, which are thought to be as magnetic size effects caused by the finite size and surface state of these particles. These behaviors are enhanced with decreasing the particle size, since the surface/volume ratio of the particle increases in the process.

In the present study, SBA-15 was prepared with controlled pore size for use as a nanoparticle synthesis template. Next, we successfully synthesized $BiMnO_3$ nanoparticles in the pores of SBA-15 and investigated their magnetic properties. It is well known that the distorted perovskite bismuth manganite $BiMnO_3$ is a multiferroic compound. Bulky $BiMnO_3$ shows ferromagnetic and ferroelectric transition at $T_M \sim 100$ K and $T_E \sim 750$ K, respectively.[12] There is an inherent coupling between the ferromagnetic and the ferroelectric ordering. Compared with the perovskite manganite $LaMnO_3$, which exhibits an A-type antiferromagnetic state with orbital ordering and superexchange interaction, $BiMnO_3$ has superexchange interaction which is responsible for the ferromagnetic state, and is subject to complex orbital ordering due to the heavily distorted MnO_6 octahedral structure.[13–15] Thus, the multiferroic property of $BiMnO_3$ strongly depends on its structure, and so its properties should suffer modification as the particle size reaches the nano level. We report here the size control of the pore of SBA-15, as well as the structure and magnetic characteristics of nanoparticles synthesized in those pores.

2. Experimental Methods

The mesoporous silica material SBA-15 was synthesized using a triblock copolymer ($EO_{20}PO_{70}EO_{20}$; average molecular weight: 5800; Aldrich) and tetraethoxysilane as the silica source.[3–5] Although various

synthesis conditions have been controlled for the systematic control of the pore size of SBA-15, in this paper we focus mainly on the reaction temperature and duration. Nanoparticles of the multiferroic material $BiMnO_3$ were synthesized in the pores of SBA-15 (pore diameter: ~8 nm) by soaking the SBA-15 in a stoichiometric aqueous solution of $BiCl_3$ and $Mn(CH_3COO)_2{\cdot}4H_2O$. Then, the soaked samples were dried and calcinated in an oxygen atmosphere at 780 ^{0}C for 18 hours. Figure 1 shows an overview of the process of nanoparticle synthesis in the one-dimensional pores of SBA-15.

Powder X-ray diffraction (XRD) measurement of SBA-15 was carried out using a laboratory X-ray diffractometer with Cu Kα radiation (PANalytical X'Pert PRO). The powder XRD measurement of the $BiMnO_3$ nanoparticles in the pores of SBA-15 and the SBA-15 were accomplished using a synchrotron radiation X-ray diffractometer at BL-1B of the Photon Factory (PF) in the Institute of Materials Structure Science, High Energy Accelerator Research Organization (KEK), Japan. These sample powders were filled into 0.5 mm diameter glass capillary. The capillary was put on a Debye-Scherrer camera with an imaging plate. The incident X-ray wavelength was 0.68791(3) Å calibrated with the CeO_2 powder diffraction pattern. The magnetic properties of $BiMnO_3$ nanoparticles were measured using a superconducting quantum interference device (SQUID) magnetometer (Quantum Design MPMS-5S).

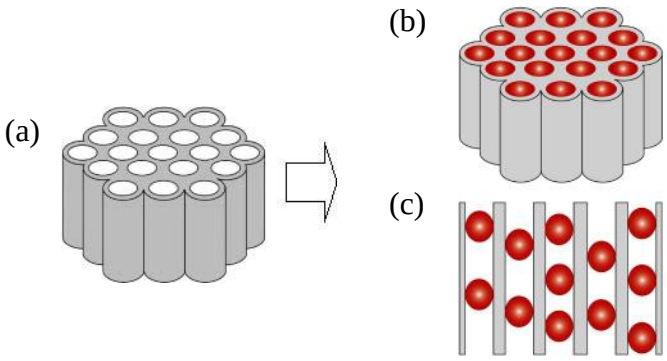

Fig. 1. (Color online) Schematics of the two-dimensional hexagonal mesostructure of SBA-15 and of nanoparticles in the pores. (a) SBA-15, (b) nanoparticles embedded in the pores of SBA-15, and (c) cross-section of (b).

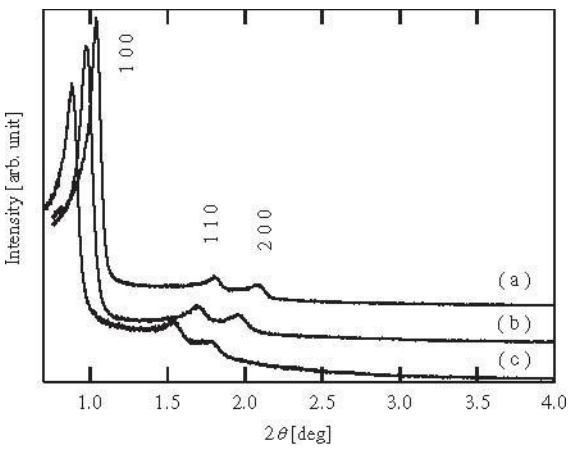

Fig. 2. XRD patterns of SBA-15 synthesized under several reaction conditions: (a) at 30 ^{o}C for 24 h, (b) at 40 ^{o}C for 48 h, and (c) at 60 ^{o}C for 48 h, respectively. The XRD was measured by Cu*K*α radiation.

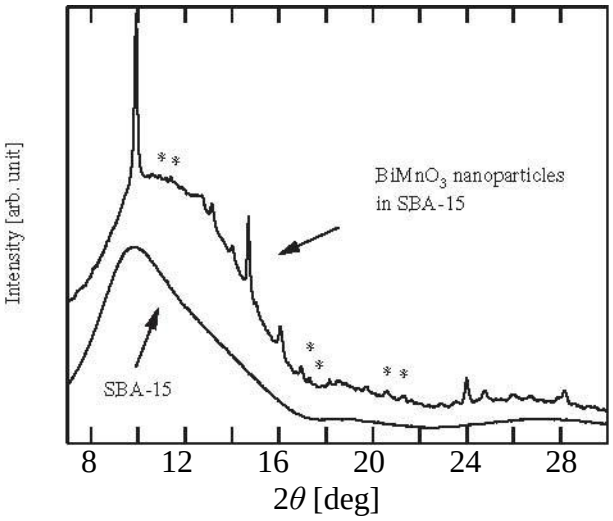

Fig. 3. XRD patterns of $BiMnO_3$ nanoparticles in the pores of SBA-15 and SBA-15 obtained by the use of synchrotron radiation. The incident X-ray wavelength was 0.68791 A˚. The asterisk indicates peaks of impurity compounds.

3. Results and Discussion

Figure 2 shows the XRD patterns of SBA-15 prepared under several synthesis conditions: the reaction temperature and duration were set to 30 ^{0}C and 24 h (a), 40 ^{0}C and 48 h (b), and 60 ^{0}C and 48 h (c), respectively. The XRD patterns showed some diffraction peaks associated with *P*6*mm* hexagonal symmetry, which indicates the formation of a well-ordered hexagonal mesopores structure. These diffraction peaks were assigned to the (100), (110), and (200) reflections of the hexagonal structure with a large unit cell. These diffraction profiles shifted toward the lower angle side with increasing synthesis temperature and duration. The *d*-spacing *d*(100) of the hexagonal structure estimated from the (100) reflection were 85, 90, and 100 A˚ for the XRD patterns (a), (b), and (c) shown in Fig. 2, respectively. The pore size is calculated by subtracting silica wall thickness from unit cell parameter of hexagonal structure. These results indicate that the pore size increased as the synthesis temperature and duration increased, since the thickness of silica wall could be controlled by the ratio of triblock copolymer to silica precursor, which is in agreement with the results of previous investigations.[3–5)]

Nanoparticles of the multiferroic material $BiMnO_3$ were synthesized in the pores of SBA-15 with a pore diameter of about 8 nm. Figure 3 shows the XRD patterns for the $BiMnO_3$ nanoparticles in the pores of SBA-15 and the SBA-15. The broad background peak at around 12 degrees in the diffraction patterns originated from the glass capillary. The diffraction pattern for the nanoparticles exhibited some Bragg peaks, which were assigned to the monoclinic structure confirmed for $BiMnO_3$ bulk crystal and the impurity phases which were considered bismuthate, BiOCl and/or Bi_2SiO_5. The average size of the nanoparticles was estimated to be about 14 nm, based on the Bragg peaks and on the results of calculations using Scherrer's equation. The obtained particle size was somewhat larger than the pore size of SBA-15. This discrepancy suggests that the nanoparticles were of spheroidal shape in the one-dimensional pores.

Figure 4 shows the temperature dependence of the DC magnetization and the inverse of the magnetic susceptibility of the $BiMnO_3$ nanoparticles in the pores of SBA-15 under an external magnetic field of H = 100 Oe. The magnetization showed ferromagnetic ordering at 98 K as determined by the peak on the dM/dT vs T curve, which was near the ferromagnetic transition temperature of $BiMnO_3$ bulk crystal. The temperature dependence of the magnetization of the $BiMnO_3$ nanoparticles suggested the coexistence of the ferromagnetic behavior similar to that of bulk crystal and antiferromagnetic behavior reproduced by Curie–Weiss law with negative Weiss temperature. The inverse magnetic susceptibility between 100 and 300K was fitted by means of the Curie–Weiss equation with a negative value, $\theta = -34$ K, as shown by the fitting solid line in Fig. 4. This indicates the presence of antiferromagnetic behavior. Compared with the Weiss temperature for $BiMnO_3$ bulk crystal, θ = 126.1 K,[16)] that for the nanoparticles deviates remarkably in sign and magnitude. The appearance of a pronounced irreversibility between field-cooled and zero-field-cooled magnetizationis attributed to blocking phenomena due to superparamagnetism. Figure 5 shows the magnetization curves at T = 5 K and 50 K. The magnetization curves do not indicate ferromagnetic

behavior, although the temperature dependence of the magnetization shows ferromagnetic ordering at 98 K. The magnetization curves for the nanoparticles are quite different from those for the bulk crystal, and give the appearance of antiferromagnetic rather than ferromagnetic behavior.

The magnetic measurement results for $BiMnO_3$ nanoparticles indicate that there is an intrinsic antiferromagnetic correlation at high temperatures, whereas at low temperatures antiferromagnetic and ferromagnetic behaviors coexist, whereas $BiMnO_3$ bulk crystal consistently shows ferromagnetic behavior. The observed behavior of the $BiMnO_3$ nanoparticles was quite different from those of usual magnetic nanoparticles, because the magnetic ordering state of nanoparticles does not usually change from that of bulk crystal. Bulky $BiMnO_3$ has superexchange interaction responsible for the ferromagnetic state and complex orbital ordering due to heavily distorted MnO_6 octahedral structure as shown in Fig. 6.[13–15] In Fig. 6, $BiMnO_3$ has six unique Mn–O–Mn superexchange pathways which consist of four ferromagnetic interactions, Mn(1)–O(1)–Mn(2), Mn(2)– O(2)–Mn(3), Mn(2)–O(3)–Mn(3), and Mn(1)–O(6)–Mn(2), and two antiferromagnetic interactions, Mn(2)–O(4)–Mn(3), and Mn(1)–O(5)–Mn(2), respectively. Three of the four ferromagnetic Mn–O–Mn angles are significantly larger than the antiferromagnetic ones.[14] In the case of pressure effects on $BiMnO_3$ bulk crystals, two components were found to coexist in a certain pressure region. The bond angle of the Mn–O–Mn pathways were enlarged by pressurization, which suggests that the competition between ferromagnetic and antiferromagnetic interaction become more pronounced with the increase in pressure and might result in frustrated glass-like or a new ferromagnetic ordered state. Pressure induced the suppression of the original ferromagnetic exchange with the simultaneous appearance of a new

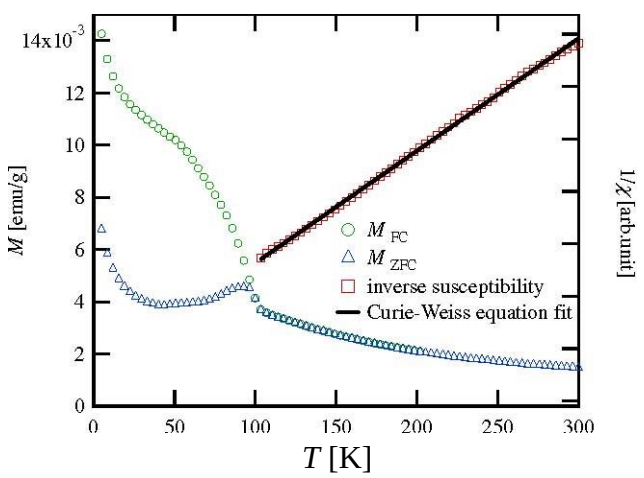

Fig. 4. (Color online) Temperature dependence of the magnetization and the inverse of susceptibility for $BiMnO_3$ nanoparticles in the pores of SBA-15 under an external magnetic field of H = 100 Oe in the field-cooled condition (circle symbols) and the zero-field-cooled condition (triangle symbols). The right axis gives the inverse susceptibility and was fitted by means of the Curie–Weiss equation as shown by the solid line.

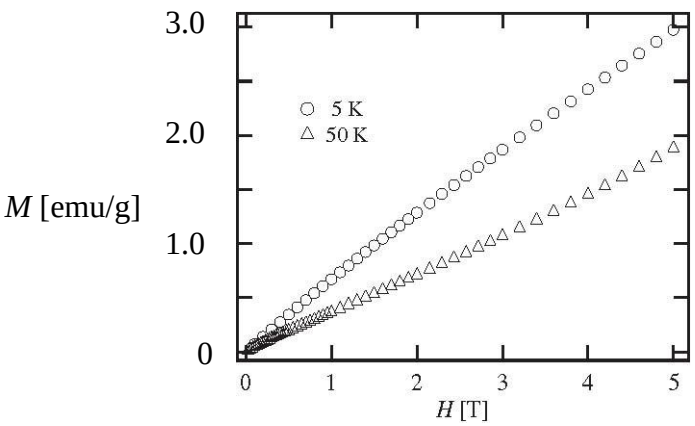

Fig. 5. Magnetization curves for $BiMnO_3$ nanoparticles in the pores of SBA-15 at 5 and 50 K.

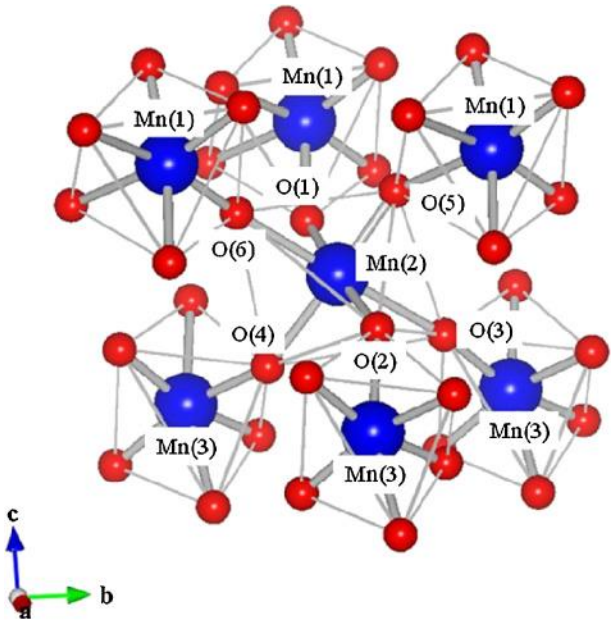

Fig. 6. (Color online) Fraction of the crystal structure of $BiMnO_3$; only MnO_6 octahedra with Mn–O bonds are given.

magnetic state.[17] In the present study, it is considered that the coexistence of ferromagnetic and antiferromagnetic behaviors was attributed to the presence of complex magnetic exchange pathways. A modification of the exchange interaction was induced by the finite size and the surface effect, which should cause the prominent appearance of antiferromagnetic behavior in nanoparticles. In the near future, detailed crystal structure analysis of nanoparticles will be carried out to investigate the modification of the Mn–O–Mn pathways.

4. Conclusions

We prepared the mesoporous silica material SBA-15 for use as a nanoparticle fabrication template, and successfully controlled its pore size. The pore size increased as the reaction temperature and duration increased. Nanoparticles of the multiferroic compound $BiMnO_3$ with an average size of about 14 nm were successfully synthesized in the pores of SBA-15, and their magnetic properties were measured. The $BiMnO_3$ nanoparticles showed unique magnetic size effects. The temperature dependence of the magnetization showed ferromagnetic behavior with a transition temperature similar to that for the bulk crystal, but the inverse susceptibility was fitted by means of the Curie–Weiss equation with a negative Weiss temperature. In addition, the magnetization curves indicated antiferromagnetic behavior. Although the magnetic measurement results for the bulk crystal consistently indicated ferromagnetic behavior, those for nanoparticles suggested that ferromagnetic and antiferromagnetic behaviors coexisted intrinsically.

1) C. T. Kresge, M. E. Leonowicz, W. J. Roth, J. C. Vartuli, and J. S. Beck: Nature 359 (1992) 710.
2) J. S. Beck, J. C. Vartuli, W. J. Roth, M. E. Leonowicz, C. T. Kresge, K.D. Schmitt, C. T. W. Chu, D. H. Olson, and E. W. Sheppard: J. Am. Chem. Soc. 114 (1992) 10834.
3) D. Zhao, J. Feng, Q. Huo, N. Melosh, G. H. Fredrickson, B. F. Chmelka, and G. D. Stucky: Science 279 (1998) 548.
4) M. Kruk and M. Jaroniec: Chem. Mater. 12 (2000) 1961.
5) V. L. Zholobenko, A. Y. Khodakov, and D. Durand: Microporous Mesoporous Mater. 66 (2003) 297.
6) T. Tajiri, H. Deguchi, S. Kohiki, M. Mito, S. Takagi, K. Tsuda, and Y. Murakami: J. Phys. Soc. Jpn. 75 (2006) 113704.
7) M. Clemente-Leo´n, E. Coronado, A. Forment-Aliaga, P. Amoro´, J. Ramı´rez-Castellanosc, and J. M. Gonza´lez-Calbet: J. Mater.Chem. 13 (2003) 3089.
8) C. Tien, E. V. Charnaya, M. K. Lee, S. V. Baryshnikov, S. Y. Sun, D. Michel, and W. Bo¨hlmann: Phys.

Rev. B 72 (2005) 104105.
9) I. V. Golosovsky, I. Mirebeau, F. Fauth, D. A. Kurdyukov, and Yu. A. Kumzerov: Phys. Rev. B 74 (2006) 054433.
10) J.-S. Jung, K.-H. Choi, Y.-K. Jung, S. H. Lee, V. O. Golub, L. Malkinski, and C. J. O'Connor: J. Magn. Magn. Mater. 272 – 276 (2004) e1157.
11) T. Tajiri, H. Deguchi, S. Kohiki, M. Mito, S. Takagi, M. Mitome, Y. Murakami, and A. Kohno: J. Phys. Soc. Jpn. 77 (2008) 074715.
12) T. Kimura, S. Kawamoto, I. Yamada, M. Azuma, M. Takano, and Y. Tokura: Phys. Rev. B 67 (2003) 180401.
13) T. Atou, H. Chiba, K. Ohoyama, Y. Yamaguchi, and Y. Syono: J. Solid State Chem. 145 (1999) 639.
14) A. Moreira dos Santos, A. K. Cheetham, T. Atou, Y. Syono, Y. Yamaguchi, K. Ohoyama, H. Chiba, and C. N. R. Rao: Phys. Rev. B 66 (2002) 064425.
15) A. A. Belik, S. Iikubo, T. Yokosawa, K. Kodama,N. Igawa, S. Shamoto, M. Azuma, M. Takano, K. Kimoto, Y. Matsui, and E. Takayama-Muromachi: J. Am. Chem. Soc. 129 (2007) 971.
16) A. A. Belikand E. Takayama-Muromachi: Inorg. Chem. 45 (2006) 10224.
17) C. C. Chou, S. Taran, J. L.Her, C. P. Sun, C. L. Huang, H. Sakurai, A. A. Belik, E. Takayama-Muromachi, and H. D.Yang: Phys. Rev.B 78 (2008) 092404.